



Analysis of mass transfer performance of micromixer device with varying confluence angle using CFD

Urooj Fatima¹ · M. Shakaib² · Inayatullah Memon¹

Received: 5 July 2019 / Accepted: 21 October 2019 / Published online: 30 October 2019
© Institute of Chemistry, Slovak Academy of Sciences 2019

Abstract

The computational fluid dynamics (CFD) study on micromixers in this paper illustrates the effect of confluence angle on mixing performance at different Reynolds numbers and flow rate ratios. The mixing performance parameters such as mixing quality and effectiveness increases with the increase in Reynolds number for all the micromixer geometries. For any value of Reynolds number, the angle of confluence is found to have a significant effect on flow behavior in the mixing channel and thus on mass transfer. The formation of vortices and the interlacing of fluid streams are identified as the favorable phenomena due to which mass transfer or mixing of fluid streams is enhanced. The mixing effectiveness is mostly observed to be high in case of unequal flow rates in the two feed/inlet channels. The optimum value of confluence angle depends of flow rate ratio. When flow rate ratio is high, T-shaped micromixer ($\theta = 180^\circ$) provides better performance while for other ratios, micromixers with relatively large angles of confluence are found more suitable.

Keywords Computational fluid dynamics · Micromixer · Confluence angle · Mixing quality

List of symbols

A	Area
c	Concentration/mass fraction (kg/kg)
d	Diameter (m)
D_{AB}	Diffusion coefficient (m ² /s)
Eu	Euler number
f	Friction factor
l	Channel length (m)
l_m	Mixing length (m)
L	Total length of channels (m)
Δp	Pressure drop (Pa)
Q	Volumetric flow rate (m ³ /s)
R	Flow rate ratio
Re	Reynolds number
x	Distance from mixing channel inlet
σ^2	Variance of concentration
α	Mixing quality
ρ	Density (kg/m ³)
u_{av}	Average velocity (m/s)

u	x -Component of velocity (m/s)
v	y -Component of velocity (m/s)
w	z -Component of velocity (m/s)
μ	Viscosity (kg/m·s)
ν	Kinematic viscosity (m ² /s)

Introduction

Due to growing popularity of microfluidic devices in various applications, extensive research has been carried out for their development and improvement in the last few decades. Large surface to volume ratio, efficient heat and mass transfer ability, high product yield and selectivity and reduced product analysis times are among the advantages of microfluidic systems (Kockmann et al. 2006; Jeong et al. 2010; Kothare 2006). The use of these devices is in biological processing, pharmaceutical industries, chemical reaction engineering, micro-scale fuel processing and non-destructive analytical applications. Several papers and articles have discussed features of these devices, applications and reviewed research done in this field (Capretto et al. 2011; Nguyen and Wu 2005; Cai et al. 2017; Nguyen and Wereley 2002).

A type/component of any microfluidic device is a passive type micromixer in which two (or more) fluids after passing through their respective inlet channels, enter and flow

✉ M. Shakaib
mshakaib@neduet.edu.pk; mshakaib@live.com

¹ Department of Chemical Engineering, NED University of Engineering and Technology, Karachi, Pakistan

² Department of Mechanical Engineering, NED University of Engineering and Technology, Karachi, Pakistan

in a common mixing channel. Small dimensions and low volumetric flowrates often keep the system in the creeping/low-laminar flow regime and mixing is considerably through molecular diffusion. The diffusion process requires long residence time and channel length to provide a homogeneous mixture. Since efficient mixing is desirable to exploit advantages of microfluidic device, various methods are employed to increase mixing rate. One method by which the mixing process can be enhanced in the passive devices is to create secondary flows by changing the geometry or by modifying the operating conditions (Garofalo et al. 2010). The secondary flows result in stretching and reorientation of the interface layer of the two segregated streams even though the overall flow system is in the laminar or steady-state regime. Numerous studies have investigated fluid dynamics and concentration profiles in microchannels of mixing devices. As examples, Kashid et al. (2011) tested various microchannel designs and showed that a caterpillar-shaped channel with structured internal surface yields better mixing performance. Hossain et al. (2009) compared zig-zag; square-wave; and curved shaped microchannel. Lowest pressure drops were found in curved-type microchannel. Ortega-Casanova and Lai (2018) performed a 2D CFD study and compared mixers with multiple inlets at different Reynolds numbers and Schmidt numbers. The results of Zhendong et al. (2012) showed that both the convergence region and the mixing channel contribute towards mixing process. The experimental work by Rahimi et al. (2017) revealed enhancement of micromixer performance through modification of micromixer's spatial shape. Another paper of Rahimi et al. (2015) indicated that the mixing effectiveness greatly depends on flow rate ratio and confluence angle. Soleymani et al. (2008) showed that the development/occurrence of vortices is related to the flow rate and the geometrical parameters of the mixer, such as the aspect ratio, the mixing angle and the throttle size. Engler et al. (2004) suggested that mixing can be enhanced by vortex formation even at low Reynolds number in micromixers. Three sub-regimes namely the stratified regime, the vortex regime and the engulfment regime within the laminar flow regime were also indicated. Lobasov et al. (2018) proposed correlations for determining the critical Reynolds number, the friction factor at different widths and heights of the mixing channel. Y-type symmetrical shaped micromixers were experimentally studied at different electric field strengths by Hsieh et al. (2013). Significant effect of Joule heating was found on mixing length. A CFD study on various types of 1–1 and 1–2 micromixer junctions was performed by Sarkar et al. (2014). Better mixing was found in the asymmetrical micromixers when compared to the symmetrical ones. Aoki et al. (2011, 2013) used the Villermaux/Dushman reaction method and showed that the channel confluence and bent improves the micromixer performance. Borgogna et al.

(2018, 2019) used a novel numerical approach to study mixing in a cross-shaped microfluidic device. The approach was suggested to result in less false/numerical diffusion effects that can be present at high Peclet numbers. The study also showed a non-monotonic variation of mixing parameters with respect to Reynolds number at low flow rate ratios. Mouheb et al. (2012) numerically and experimentally studied flow in T-shaped and cross-shaped micromixers. The results revealed that when Reynolds number is increased, flow becomes three-dimensional in the outlet channels. The review of the papers indicate that the geometrical factors such as shape of mixer, dimensions and confluence angle and fluid/flow parameters like Reynolds number, flow rate ratios and mass diffusivity greatly affect the mixing efficiency of the microfluidic devices. In this paper, we study the effect of confluence angle which is the angle between two inlet channels. To the authors' knowledge, the effect of this parameter has not been investigated in detail and in the wide range ($30\text{--}330^\circ$) as considered in this research work. The flow behavior in terms of velocity and vorticity and concentration/mixing patterns has been discussed at different values of flow rate ratio and Reynolds number. The Reynolds number in this study is in the regime in which vortex or engulfment flow exists which is the typical flow regime in the micromixer devices.

Modeling procedure

CFD simulations are carried out for predicting mixing characteristics in microchannels with different angles. The schematic diagram of the geometry constructed for the 3D simulations is shown in Fig. 1. It consists of two inlet channels and a mixing/outlet channel. For all the geometries, the diameter d and the channel lengths l are equal to 0.5 mm and 15 mm, respectively. The tracer fluid flows in horizontal channel A of the micromixer while water flows in channel B whose inclination/angle is varied. The angle θ measured with respect to $+y$ axis (or channel A) in the counterclockwise direction is the confluence angle. θ is varied with an interval of 30° to allow systematic analysis for the effect of this parameter on the mixing process.

For meshing, the computational region is divided into two connected volumes as shown in Fig. 2. In the central portion which is the junction/mixing zone, an unstructured mesh is created due to the complexity of the geometry while the remaining portions of the three channels contain the structured mesh. The mesh is more refined in the mixing zone as can be seen in Fig. 2, where high gradients of local velocities and concentrations are expected. A grid containing about 8×10^5 control volumes is considered to be sufficient and is found to provide grid-independent solution. The comparison for two geometries given in Fig. 3 shows that the mixing

Fig. 1 Schematic diagram of a microchannel device (θ : confluence angle, d diameter of circular channels)

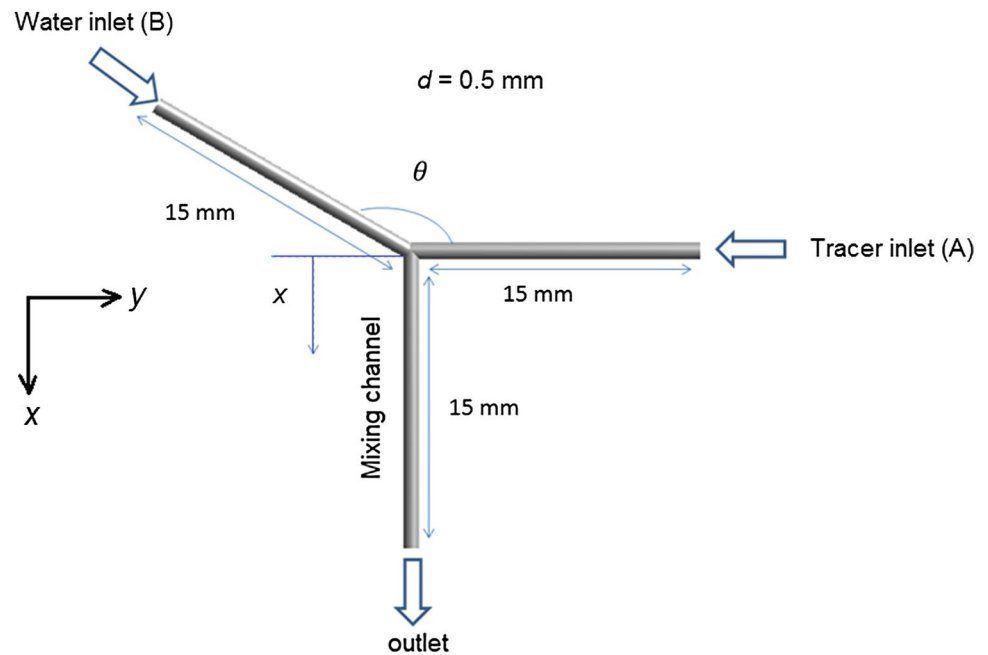
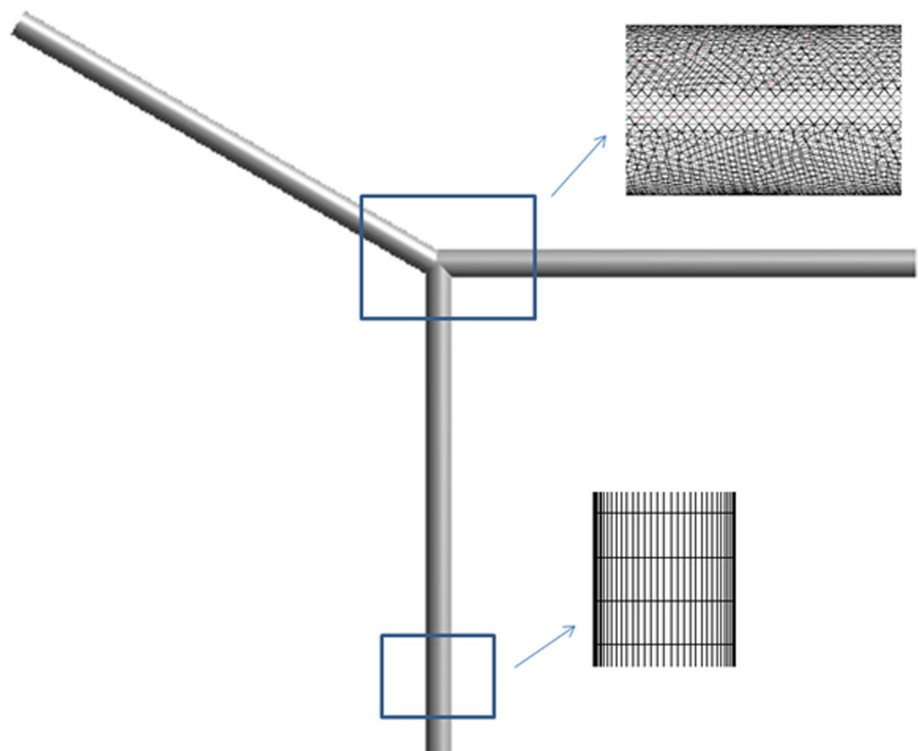


Fig. 2 Computational mesh for a microchannel mixer



quality [as defined in Eq. (8)] initially varies when number of cells is increased. The variation becomes insignificant when number of cells is greater than 8×10^5 . For a T-shaped microchannel, the difference of mixing qualities at the outlet cross section at two grids (8×10^5 cells and 1.4×10^6 cells) is found less than 1.5% indicating that the created grid is suitable.

The two fluids are assumed as Newtonian with identical physical properties. The value of density ρ is 998 kg/m^3 and viscosity μ is $0.001 \text{ kg/m}\cdot\text{s}$. The diffusivity D_{AB} of tracer solution in water is taken as $1.5 \times 10^{-9} \text{ m}^2/\text{s}$ (Fang et al. 2012).

The microchannel device is assumed to be in horizontal position and the effect of gravity is ignored. Boundary

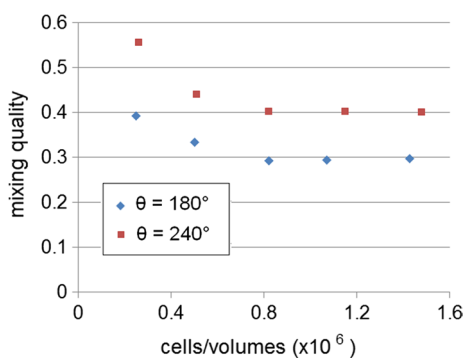


Fig. 3 Mixing quality versus number of cells ($Re = 260$)

conditions for the circular inlets and the outlet are velocity inlet and pressure outlet, respectively. The curved surfaces of the three channels and the mixing/junction zone are assumed wall. The governing equations are the continuity, the momentum and the concentration equations for steady laminar flow and species transport without reaction as given in Eqs. (1–5):

$$u \frac{\partial u}{\partial x} + v \frac{\partial v}{\partial y} + w \frac{\partial w}{\partial z} = 0, \quad (1)$$

$$u \frac{\partial u}{\partial x} + v \frac{\partial u}{\partial y} + w \frac{\partial u}{\partial z} = -\frac{1}{\rho} \frac{\partial p}{\partial x} + \nu \left(\frac{\partial^2 u}{\partial x^2} + \frac{\partial^2 u}{\partial y^2} + \frac{\partial^2 u}{\partial z^2} \right), \quad (2)$$

$$u \frac{\partial v}{\partial x} + v \frac{\partial v}{\partial y} + w \frac{\partial v}{\partial z} = -\frac{1}{\rho} \frac{\partial p}{\partial y} + \nu \left(\frac{\partial^2 v}{\partial x^2} + \frac{\partial^2 v}{\partial y^2} + \frac{\partial^2 v}{\partial z^2} \right), \quad (3)$$

$$u \frac{\partial w}{\partial x} + v \frac{\partial w}{\partial y} + w \frac{\partial w}{\partial z} = -\frac{1}{\rho} \frac{\partial p}{\partial z} + \nu \left(\frac{\partial^2 w}{\partial x^2} + \frac{\partial^2 w}{\partial y^2} + \frac{\partial^2 w}{\partial z^2} \right), \quad (4)$$

$$u \frac{\partial c}{\partial x} + v \frac{\partial c}{\partial y} + w \frac{\partial c}{\partial z} = D_{AB} \left(\frac{\partial^2 c}{\partial x^2} + \frac{\partial^2 c}{\partial y^2} + \frac{\partial^2 c}{\partial z^2} \right). \quad (5)$$

The equations are solved using CFD code ANSYS Fluent. Second order upwind scheme is used for discretization of the momentum and the concentration/mass transfer equations. In order to couple pressure and velocity fields, SIMPLE (semi-implicit method for pressure linked equations) algorithm is used (Patankar and Spalding, 1972). The convergence limit for the residuals of continuity, velocity components and mass fraction is set as 10^{-5} .

The effect of confluence angle is determined on mixing characteristics at different Reynolds numbers and flow rate ratios.

The Reynolds number is defined as:

$$Re = \frac{u_{av} d}{\nu}, \quad (6)$$

where u_{av} is the average velocity in the mixing (outlet) channel, d is the diameter of the channel and ν is kinematic viscosity. Simulations are carried out at Reynolds number (Re) of 130, 195 and 260 that are typical values for flow in micromixing units.

Flow rate ratio R is defined as:

$$R = \frac{Q_B}{Q_A}, \quad (7)$$

where Q_B is the flow rate of water and Q_A is the flow rate of tracer solution. The values of R considered are 0.5, 1, 2 or 3 at $Re = 195$.

In order to determine mass transfer performance of mixing devices, several models have been used by researchers (Vatankhah and Shamloo 2018). A parameter often used to estimate micromixer efficiency is mixing quality α which is given in Eq. (8):

$$\alpha = 1 - \sqrt{\frac{\sigma^2}{\sigma_{max}^2}}, \quad (8)$$

where σ is variance at any plane and σ_{max}^2 is the maximum possible variance in concentration (e.g., in case of symmetrical boundary conditions $\sigma_{max}^2 = 0.25$). In Eq. (8) $\alpha = 0$ (or $\sigma = \sigma_{max}^2$) means no mixing that is the two fluids are segregated. On the other hand, $\alpha = 1$ means complete mixing which can be achieved after a sufficiently large distance/length. Both α and σ are functions of x since the concentration gradients or variance reduces and the mixing quality increases as the two fluids move in the mixing channel.

The values of variance (σ) can be obtained by simply taking average of the squared differences of mass fraction at various grid points from the mean mass fraction (e.g., Engler et al. 2004; Vatankhah and Shamloo 2018) or can be weighted using cell areas (Aoki et al. 2011), cell volumes (Lobasov et al. 2018) or azimuthal velocity (Garofalo et al. 2010). Though the different methods lead to different numerical values of mixing quality or efficiency, for comparison of the various confluence angles any of the method will be suitable. In this paper, σ is estimated using area weighted relation given as:

$$\sigma = \sqrt{\frac{\sum_{i=1}^n A_i (c_i - \bar{c})^2}{A_{total}}}. \quad (9)$$

In the above equation c_i is the concentration/mass fraction of tracer in the i th cell, \bar{c} is the average mass fraction of tracer in the cross-sectional plane, A_i is the area of cell i and A_{total} is the total area of the plane and n is the number of cells in the cross section.

Though better mixing is desirable, it is usually at the expense of high pressure drop or power requirement. A

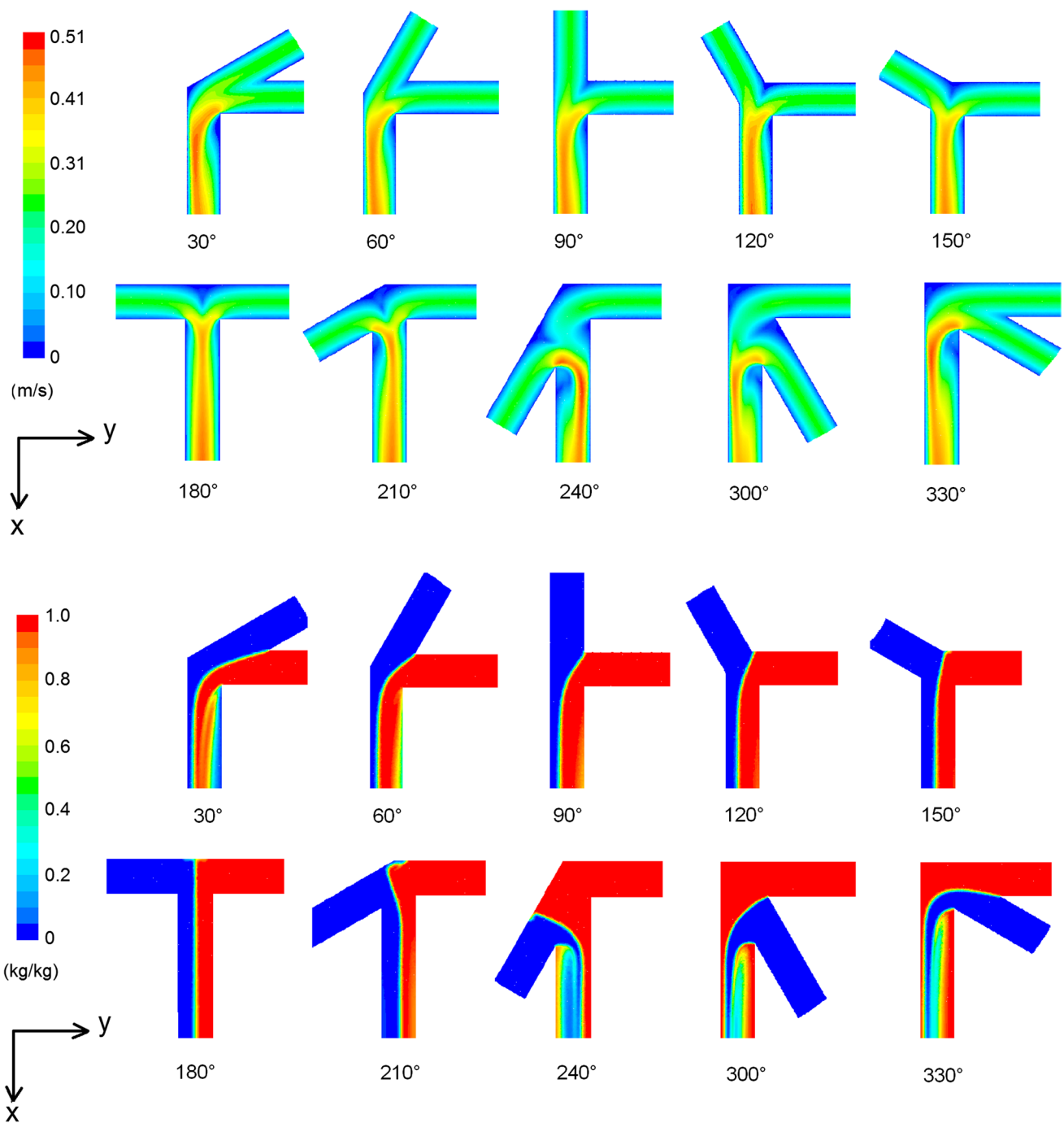


Fig. 4 Contours of velocity and concentration/mass fraction of tracer at different confluence angles ($Re = 130, R = 1$)

dimensionless parameter termed as ‘Mixing effectiveness’ ME and given in Eq. (10) can also be used as a performance indicator for micromixer device (Kockmann et al. 2006):

$$ME = \frac{d}{l_m} \frac{1}{Eu} \tag{10}$$

In Eq. (10) Eu is Euler number ($(\Delta p / \rho u^2)$) and l_m is the mixing length. Because of the geometric similarity, all

microchannels have same diameter and due to short length of the outlet channel, the mixing length cannot be easily calculated. A modified relation for mixing effectiveness ME' , therefore, as given in Eq. (11) may be used (Rahimi et al. 2015). A high value of ME' indicates high mixing rate per unit (dimensionless) pressure drop:

$$ME' = \frac{\alpha}{Eu} \tag{11}$$

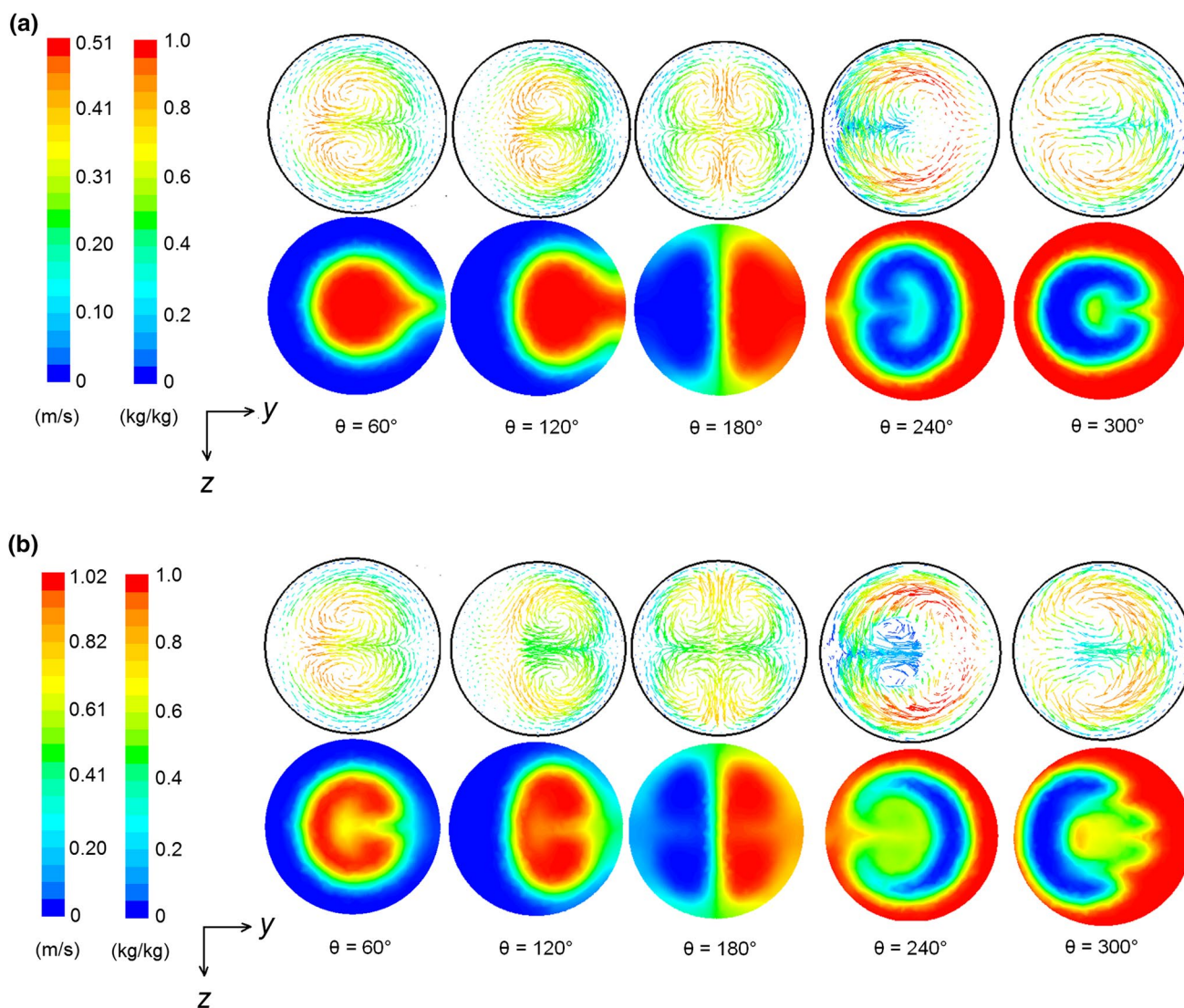


Fig. 5 Velocity profiles and mass fraction contours in micromixers (at $x=1$ mm) **a** $Re=130$ **b** $Re=260$

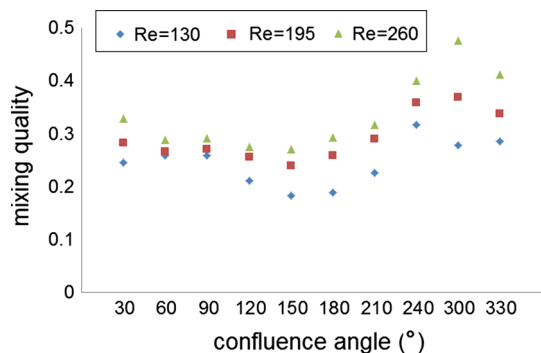


Fig. 6 Mixing quality (at outlet section) versus confluence angle at different Reynolds number

For comparison of pressure drop values with previously published papers, friction factor f is determined using Eq. (12):

$$f = \frac{\Delta p d}{L} \frac{2}{\rho u_{av}^2}. \quad (12)$$

Results and discussion

The velocity and concentration/mass fraction contours at different confluence angles θ are shown in Fig. 4. Reynolds number is 130 while the flow rate ratio is 1 for all the geometries. The velocity profiles indicate general flow features such as formation of high and low velocity regions as two fluids enter into the mixing channel. High-velocity region

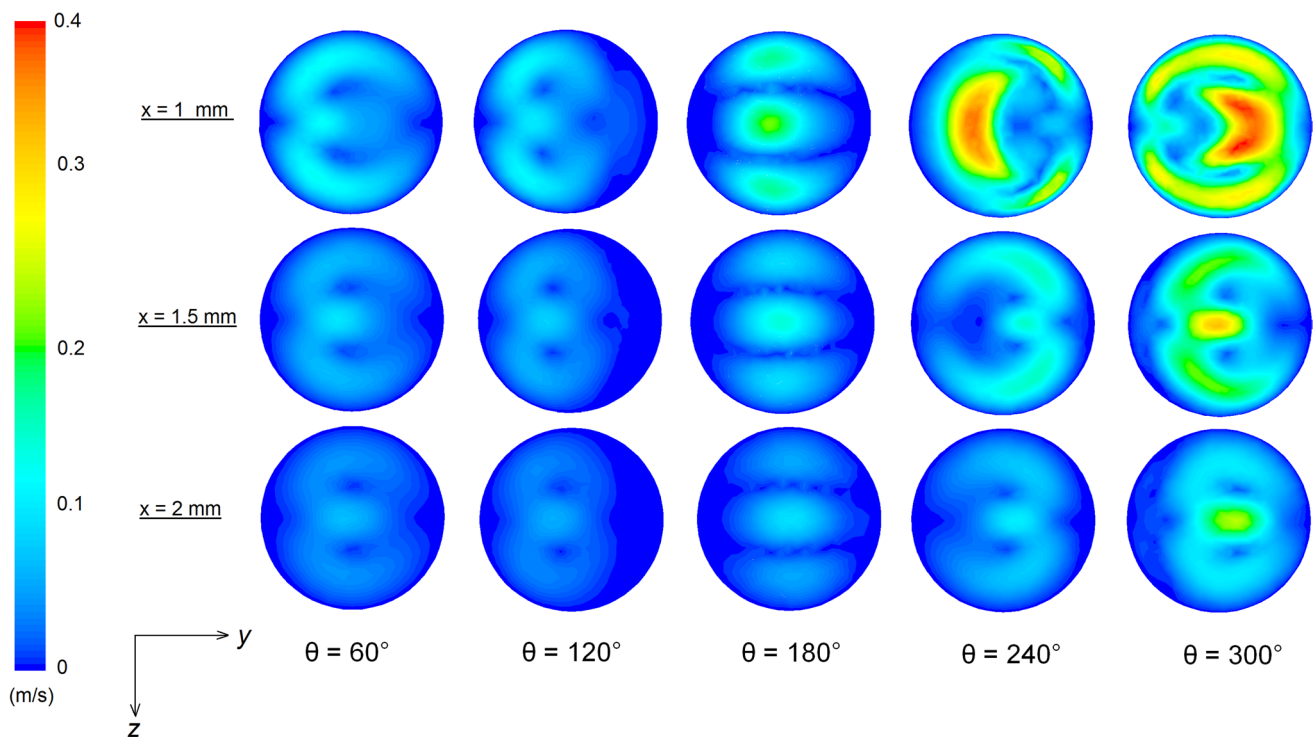


Fig. 7 Contours of velocity u_{yz} at $x = 1, 1.5$ and 2 mm ($Re = 260, R = 1$)

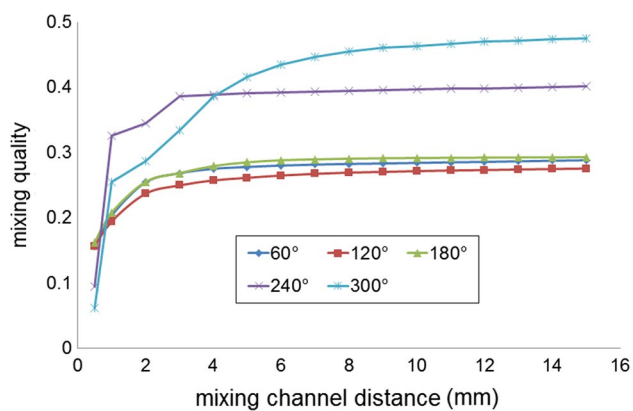


Fig. 8 Variation of mixing quality with respect to mixing channel length ($Re = 260$)

exists as a result of increased mass flux in the mixing channel, whereas low velocity portion is due to flow separation and recirculation. The high-velocity zone in some geometries such as with low confluence angles ($30\text{--}120^\circ$) occur in the left portion of the outlet/mixing channel. The low velocity (flow recirculation) region is on the opposite side that is in the right portion. The location and size of the two different regions (high and low velocity) change with the confluence angle. In addition to low velocity zone at the entrance location of mixing channel, a low velocity zone

also exists at the top portion of the device which is noticeable at large values of θ .

The concentration profiles show that at $\theta = 30^\circ$, the tracer concentration is high in the center of the mixing channel while water fills the outer portion. With the increase of angle, water tends to flow in the left portion while the tracer fills the right portion of the mixing channel. In some geometries such as when $\theta = 120^\circ$ or 180° , water and tracer appear to flow as separate streams with little mixing. When the angle is greater than 180° , water fluid moves upwards in inlet channel and then downwards into the mixing tube. This major turn in flow path can enhance the rotational movement in the mixing region. When $\theta = 240\text{--}330^\circ$ local concentration values vary significantly in horizontal/transverse plane (y -direction). This is due to increased size of low velocity/recirculation zone seen in velocity contours. The formation of large-sized recirculation zones in the mixing channel causes the two fluids to move slowly while they come in contact and also increases the contact surface area of the two fluids. The flow recirculation also increases the residence time of fluids which ultimately leads to high mixing rates.

The flow behavior and concentration variation in xy plane are shown in Fig. 4. To determine the 3D flow characteristics, the velocity vectors and mass fraction contours are shown in Fig. 5 in yz direction at a plane 1 mm from the entrance of the mixing channel. Although the main flow is

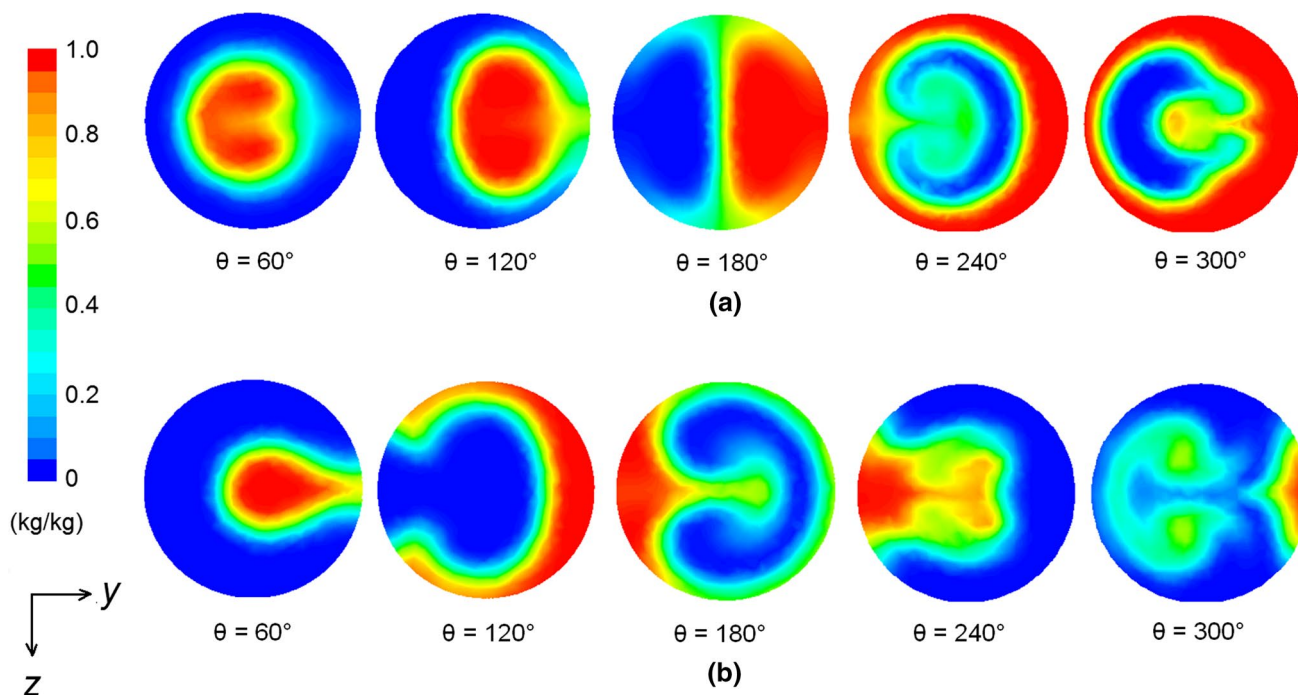
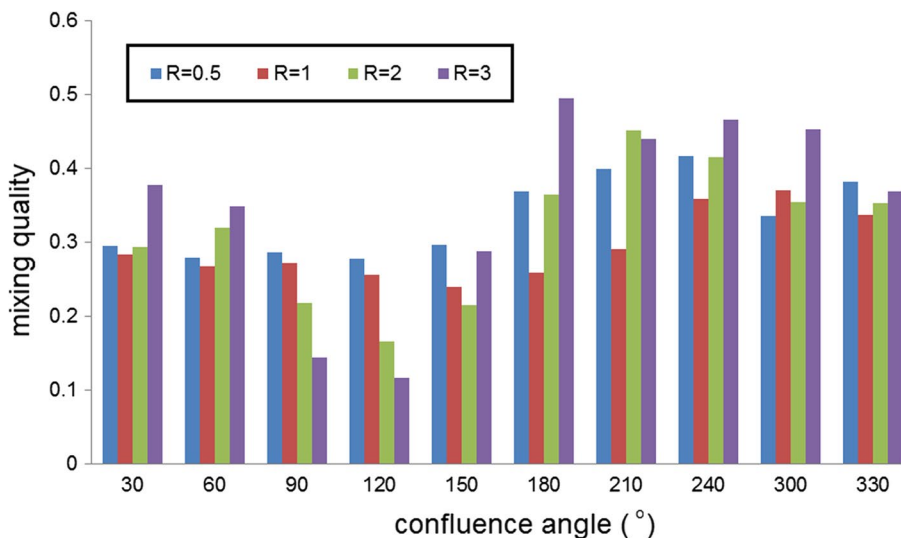


Fig. 9 Effect of flow rate ratio on mass fraction distribution **a** $R = 1$ **b** $R = 3$ ($Re = 195$, $x = 1$)

Fig. 10 Mixing quality at outlet for different θ at different flow rate ratios ($Re = 195$)



in the axial direction, the plot of velocity vectors in the figure shows considerable fluid movement in transverse cross-sectional plane and formation of vortices. As expected, the geometry with angle of 180° results in symmetrical flow and concentration patterns. The comparison of mass fraction contours shows that when Reynolds number is low, relatively distinct regions of water and tracer fluids are present in most of the geometries. The variation in mass fraction is only seen at the interface/contact surface of the two fluids which means less mixing. When Reynolds number is increased,

the variation of concentration is fairly continuous due to more mixing. In cases of confluence angles of 240° or 300° , it appears from mass fraction contours that the tracer fluid encloses the water stream. This indicates better diffusion of one fluid into the other. At small angles ($\theta = 60^\circ$ or 120°) the two fluids flow as isolated streams with less mixing. In some regions, velocity vectors are not visible, for example, at angles of 120° and 240° , meaning that flow direction is axial at that particular location.

Table 1 Magnitude of x -vorticity at $x = 1$ mm in different micromixers

θ (°)	$Re = 130, R = 1$	$Re = 195, R = 0.5$	$Re = 195, R = 1$	$Re = 195, R = 2$	$Re = 195, R = 3$	$Re = 260, R = 1$
30	294.9	752.9	630.2	751.7	695.8	1013.8
60	236.5	723.8	523.4	409.5	430.0	856.0
90	199.1	742.8	455.3	191.4	116.7	757.3
120	160.3	752.6	401.1	277.4	358.5	701.4
150	153.2	778.3	436.8	561.9	781.8	805.0
180	177.8	862.9	523.4	855.6	1014.7	973.8
210	243.1	954.6	651.2	1028.3	1169.8	1090.5
240	667.2	775.7	1239.0	2166.3	2486.6	2118.1
300	916.2	1438.9	2015.4	2442.1	2668.3	3443.9
330	407.8	874.0	876.1	952.5	1032.3	1470.9

Mixing quality as calculated from Eq. (8) is shown in Fig. 6 for the three Reynolds number. The mass transfer is found to be a direct function of Reynolds number as the mixing quality increases with the increase in Reynolds number at all confluence angles. When confluence angle θ is between 60° and 150° , low mixing qualities are obtained. High mixing qualities are seen when θ is 240 – 330° . The possible reason is that at small angles, the fluid elements rotation is not significant in the mixing region. When the value of angle θ is large, relatively strong flow circulation in the junction region enhances the mixing. On the overall basis, the micromixers with large angles can thus be considered better in terms of mass transfer performance. At high Reynolds number, rapid increase in mixing rate can be due to change of flow regime from vortex to engulfment. In engulfment regime, the rotational movement of fluids plays a major role in enhancing the mixing process.

In order to explain how the flow behavior changes in the mixing channel, contours of velocity component in yz plane ($\mathbf{u}_{yz} = (v^2 + w^2)^{1/2}$) are obtained and shown at different cross-sectional planes in Fig. 7. Due to presence of recirculation regions as seen in Fig. 5, non-axial velocity component is noticed to be significant at certain locations at $x = 1$ mm. As the fluid proceeds, the strength of recirculation reduces and the direction becomes more axial which reduces the magnitude of \mathbf{u}_{yz} . In micromixers with large values of θ , the \mathbf{u}_{yz} component of velocity is high which means significant rotational flow at the entrance plane of the mixing channel. From the contours in Fig. 7, it can be inferred that the radial/transverse components of velocity (or \mathbf{u}_{yz}) considerably reduce after 2–3 mm depending upon the confluence angle. The flow can therefore be assumed axial after this distance.

The variation of mixing quality versus length can be seen in Fig. 8. It shows that mixing mainly occurs at the entrance of outlet channel where two fluids come in contact. Approximately after 3 mm, the rise in mixing quality becomes gradual and the fluids continue to flow in remaining portion of channel without any major change in local concentrations.

The effect of flow rate ratio (R) is also studied and the mass fraction contours at different confluence angles are shown in Fig. 9. The comparison for angle 60° shows that when flow ratio is 1, water fills the outer portion of the channel while tracer is in center. The increase in water flow rate (or ratio), causes the tracer fluid to shift towards the right wall of the channel. A similar effect of R is found when $\theta = 120^\circ$. Water fills mostly the left and central portion at high flow rate ratio while tracer sticks to right and the outer portion. When angle is 180° or 240° , at $R = 3$, water (which is initially in the left inlet channel) occupies right portion of the mixing channel. This means considerable mixing of the two fluids. The mass fraction profiles for geometry with $\theta = 300^\circ$ also appear to be suitable at high flow ratio as continuous variation in local mass fraction values are found indicating high mixing rates.

The mixing quality α calculated at the outlet section is shown for the micromixers in Fig. 10. On overall basis, when angle θ is between 90° and 150° , low mixing qualities are obtained. The comparison of mixing qualities at different flow ratios show that mixing improves due to unequal flow ratios. The fluids layers intertwine more when flow rates are unequal. The figure also suggests that the optimal value of confluence angle also depends on the flow rate ratio. The optimal angles are 240° , 300° , 210° and 180° at flow rate ratios of 0.5, 1, 2 and 3, respectively.

The increase/decrease of the mixing qualities can also be related to x -vorticity values as given in Table 1. The vorticity increases with the increase in Reynolds number due to high local velocities. As seen for mixing qualities in Fig. 10, vorticity values are generally found low when confluence angles θ are small and unequal flow rates increases vorticity in most of the cases. In some geometries, however, increase in flow rate ratio decrease vorticity (e.g., $\theta = 90^\circ$ or 120°) due to better streamlining of flow in these cases at high values of R .

The flow patterns are shown in Fig. 11 with the help of velocity vectors to explain further the mixing process. The figure shows that when Reynolds number is low

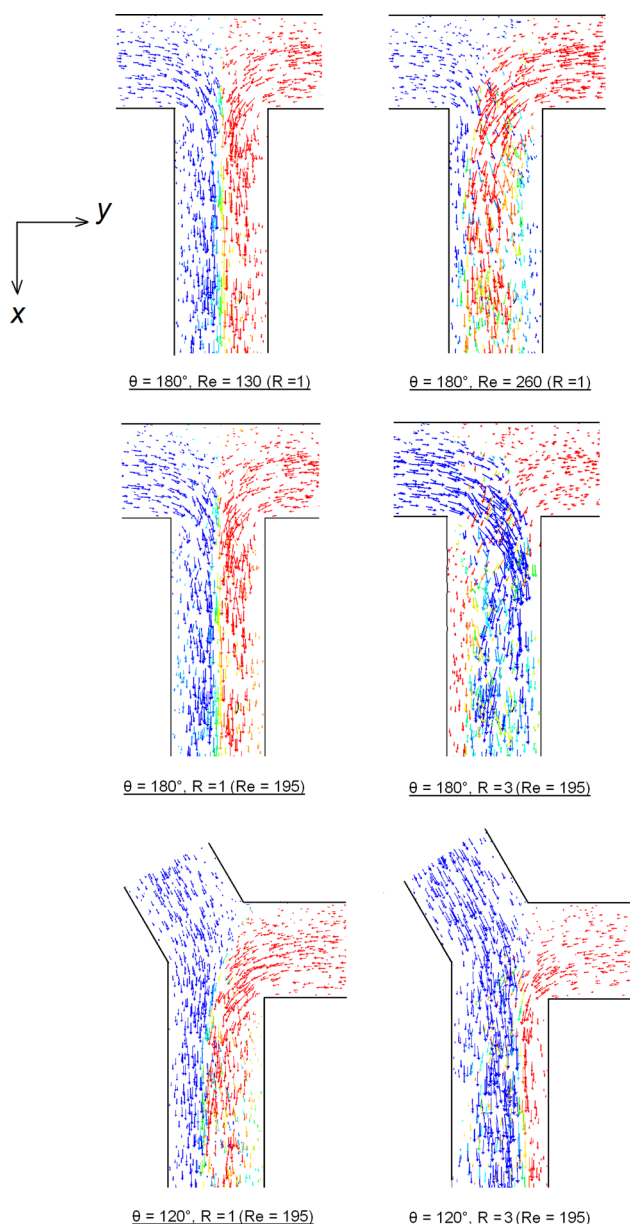


Fig. 11 Flow pattern for different values of R and Re (red: tracer, blue: water)

($Re = 130$), water and tracer follow well-defined separate paths. At high Reynolds number, the flow paths of two fluids interlace with each other. The mixing quality, thus, increases at high Reynolds number (as observed in Fig. 6). The increase in flow rate ratio can improve the mixing phenomenon such as in a T-shaped geometry ($\theta = 180^\circ$) or can reduce like in the case of angle $\theta = 120^\circ$. In the T-shaped micromixer, when flow rates are equal, the fluids appear to maintain the vertical/axial direction in the outlet channel. When $R = 3$, water follows a curved path and interacts with the tracer fluid layers. In the micromixer with $\theta = 120^\circ$, at a high flow rate ratio (i.e., $R = 3$), the

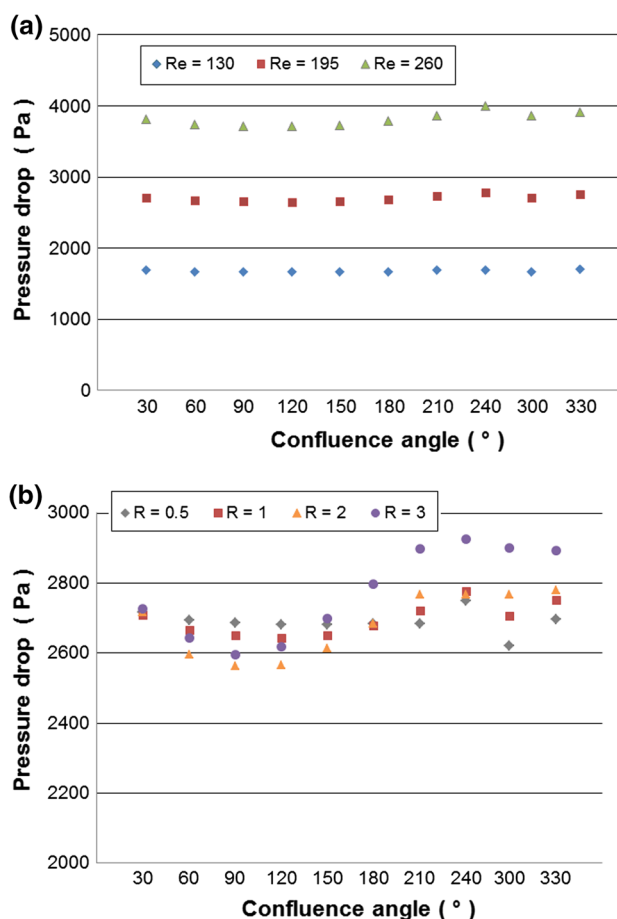


Fig. 12 Pressure drop at different **a** Reynolds number ($R = 1$), **b** flow rate ratios ($Re = 195$)

high-velocity water stream squeezes the tracer fluid layers without any major mixing.

A desired feature for any flow device is that it results in less pressure loss (Δp). The various geometries are therefore compared based on inlet pressure requirement as depicted in Fig. 12. As can be anticipated, Δp increases with the increase in Reynolds number. The effect of confluence angle on pressure drop is not much significant when Reynolds number or flow rate ratio is low. The Δp values vary less than 5% at various angles in these cases. When $R > 1$ or $Re = 260$, pressure drops are found to be 10–15% higher in geometries with $\theta > 180^\circ$. The reason is that when $\theta > 180^\circ$, water takes a sharp turn to move into the mixing channel. This requires more pressure force particularly when water flow rate is high.

Mixing effectiveness (ME') is calculated using Eq. (11) and plotted in Fig. 13. Similar to the mixing quality, the effectiveness ME' increases with the increase in Reynolds number. The appropriate geometries/confluence angles depend on flow rate ratio and Reynolds number. When flow rate ratio is 0.5, high effectiveness values are found when

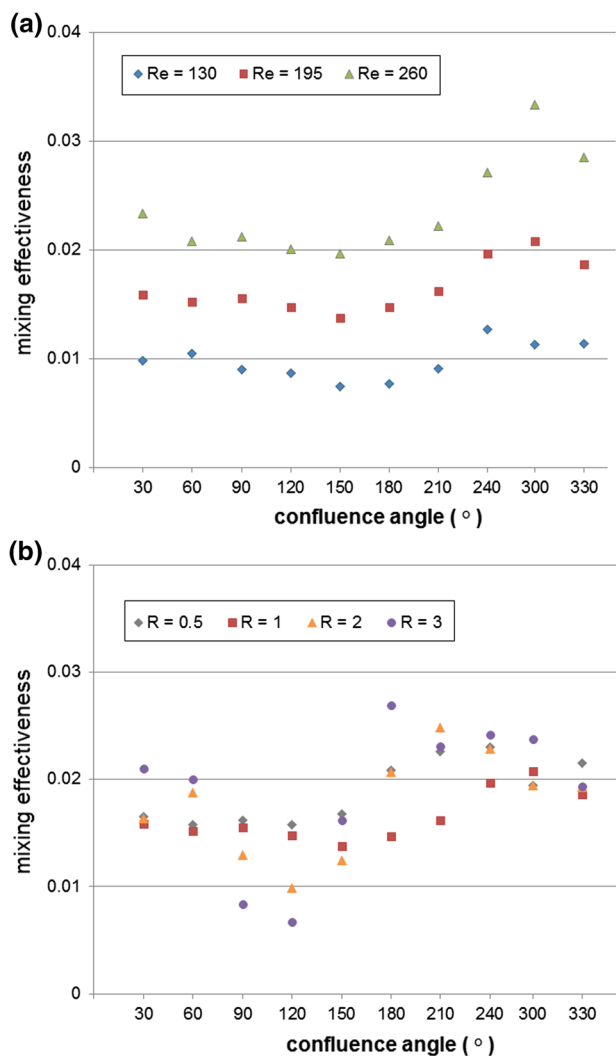


Fig. 13 Mixing effectiveness at different **a** Reynolds number ($R=1$), **b** flow rate ratios ($Re=195$)

θ is 210–240°. For flow rate ratio of 1, the peak value of ME' is seen in range 240–330°. When flow ratios are 2 or 3, mixing effectiveness initially decreases and then increases with the increase in confluence angle. This is due to low mixing qualities seen for angles in the range of 60–150° in Fig. 10. The peak values of ME' are achieved at 210° and 180°, respectively. The geometries with $\theta \geq 180^\circ$, hence, are found better for micromixer devices due to superior mass transfer performance.

To assess the reliability of the present CFD study, the results are compared qualitatively and quantitatively with the findings in other papers. Engler et al. (2004) studied a T-shaped micromixer at different Reynolds number and determined mixing quality at a location of 1.8 mm down the mixing channel. The comparison at a Reynolds number of 195 shows that in present work, mixing quality is 22.2%, whereas in the work of Engler et al. this value was around

28% at the same location. Similarly, Mouheb et al. (2012) calculated mixing quality at a distance of $x=5.5d$ for a T-shaped microchannel. The reported mixing quality at this plane was 23% while in the present research this value is 24.7%. A comparison of mass fraction contours obtained through simulations is done with the work of Rahimi et al. (2015) in which dye spreading was observed through visualization experiments at different flow rate ratios. The mass fraction contours and experimental images are shown in Fig. 14. The comparison shows similarity of mass fraction profile of tracer predicted through CFD with the dye flow pattern for various flow rate ratios. The reasonable agreement in qualitative terms also indicates accuracy of present numerical results. A comparison is also done in terms of pressure drop/friction factor. Friction factors are calculated using Eq. (12) for T-type micromixer at different Reynolds numbers. The friction factors obtained in this paper and friction factors determined experimentally by Aoki et al. (2013) are given in Fig. 15. The figure shows that the present results over-predict the friction factors. However, the differences are less than 20% which can again be considered acceptable.

Conclusion

The fluid flow and mass transfer analysis in this work shows considerable influence of confluence angle θ on velocity, mass fraction/concentration distribution thereby affecting the performance of micromixers. The angle θ alters the fluid dynamics in mixing zone which in turn affects the mixing performance. The formation of recirculation zones and increase in magnitude of transverse/radial components of velocity leads to high mixing rates. The flow pattern and thus the mixing, in addition to angle θ , also depend on Reynolds number and flow rate ratio. The results of mixing parameters do not indicate simple increasing and decreasing trend with θ and R as flow structure in the mixing zone modifies with variation of any of these parameters. Usually low mixing qualities are observed when θ is in range of 90–150° and high mixing performance is found when θ is greater than 180°. For many of the micromixers, high flow rate ratio results in high mixing rates as water pathlines/vectors interlace more with the tracer fluid layers. The T-shaped micromixer which has an angle of 180° gives maximum mixing quality when flow rate ratio is 3. The geometrical and flow parameters considered also affect the pressure losses in the microchannel device. When Reynolds number is increased from 130 to 260, pressure drop increases about 100%. With the variation of flow rate ratio for a given Reynolds number and for a given geometry, the pressure drop values remain within 15%. Pressure drop is found

Fig. 14 Comparison of mass fraction contours with dye spreading experimental results by Rahimi et al. (2015)

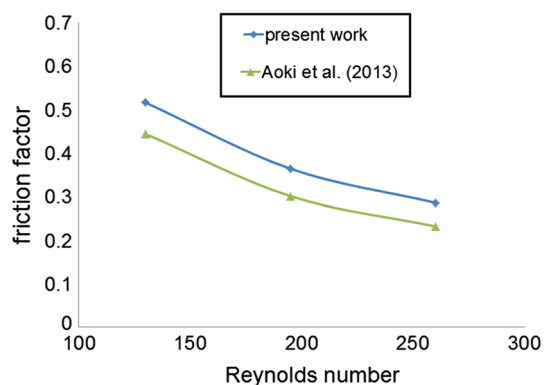
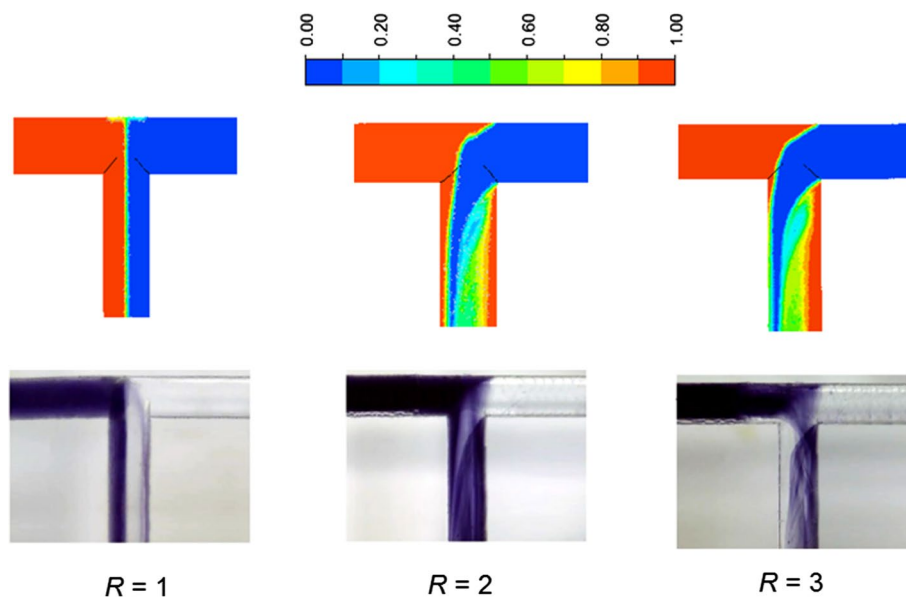


Fig. 15 Comparison of friction factor with the work of Aoki et al. (2013) for a T-shaped microchannel

to be high in micromixers with large confluence angles particularly at high values of flow rate ratio. The mixing effectiveness also increases with Reynolds number. The optimum confluence angles based on mixing effectiveness are identified in the range of 180–330°. Finally, the present simulation results fairly agree with previous computational and experimental studies.

Acknowledgements The support provided by NED University of Engineering and Technology, Karachi, Pakistan, is acknowledged.

Compliance with ethical standards

Conflict of interest On behalf of all authors, the corresponding author states that there is no conflict of interest.

References

- Aoki N, Umei R, Yoshida A, Mae K (2011) Design method for micromixers considering influence of channel confluence and bend on diffusion length. *Chem Eng J* 167:643–650
- Aoki N, Fukuda T, Maeda N, Mae K (2013) Design of confluence and bend geometry for rapid mixing in microchannels. *Chem Eng J* 227:198–202
- Borgogna A, Murmura MA, Annesini MC, Giona M, Cerbelli S (2018) Inertia-driven enhancement of mixing efficiency in microfluidic cross-junctions: a combined Eulerian/Lagrangian approach. *Microfluid Nanofluid* 22:20
- Borgogna A, Murmura MA, Annesini MC, Giona M, Cerbelli S (2019) A hybrid numerical approach for predicting mixing length and mixing time in microfluidic junctions from moderate to arbitrarily large values of the Péclet number. *Chem Eng Sci* 196:247–264
- Cai G, Xue L, Zhang H, Lin J (2017) A review on micromixers. *Micromachines* 8:274
- Capretto L, Cheng W, Hill M, Zhang X (2011) Micromixing within microfluidic devices. *Top Curr Chem* 304:27–68
- Engler M, Kockmann N, Kiefer T, Woias P (2004) Numerical and experimental investigations on liquid mixing in static micromixers. *Chem Eng J* 101:315–322
- Fang Y, Ye Y, Shen R, Zhu P, Guo R, Hu Y, Wu L (2012) Mixing enhancement by simple periodic geometric features in microchannels. *Chem Eng J* 187:306–310
- Garofalo F, Adrover A, Cerbelli S, Giona M (2010) Spectral characterization of static mixers. The S-shaped micromixer as a case study. *AIChE J* 56(2):318–335
- Hossain S, Ansari MA, Kim K (2009) Evaluation of the mixing performance of three passive micromixers. *Chem Eng J* 150:492–501
- Hsieh SS, Lin JW, Chen JW (2013) Mixing efficiency of Y-type micromixers with different angles. *Int J Heat Fluid Flow* 44:130–139
- Jeong GS, Chung S, Kima CB, Lee SH (2010) Applications of micro-mixing technology. *Analyst* 135:460–473
- Kashid M, Renken A, Kiwi-Minsker L (2011) Mixing efficiency and energy consumption for five generic microchannel designs. *Chem Eng J* 167:436–443

- Kockmann N, Kiefer T, Engler M, Woias P (2006) Convective mixing and chemical reactions in microchannels with high flowrates. *Sens Actuators B* 117:495–508
- Kothare MV (2006) Dynamics and control of integrated microchemical systems with application to micro-scale fuel processing. *Comput Chem Eng* 30:1725–1734
- Lobasov AS, Minakov AV, Kuznetsov VV, Rudyak VY, Shebeleva AA (2018) Investigation of mixing efficiency and pressure drop in T-shaped micromixers. *Chem Eng Process* 134:105–114
- Mouheb NA, Malsch D, Montillet A, Solliec C, Henkel T (2012) Numerical and experimental investigations of mixing in T-shaped and cross-shaped micromixers. *Chem Eng Sci* 68:278–289
- Nguyen NT, Wereley ST (2002) *Fundamentals and applications of microfluidics*, vol 2. Artech house, Norwood
- Nguyen N-T, Wu Z (2005) Micromixers: a review. *J Micromech Microeng* 15:1–16
- Ortega-Casanova J, Lai C-H (2018) CFD study about the effect of using multiple inlets on the efficiency of a micromixer. Assessment of the optimal inlet configuration working as a microreactor. *Chem Eng Process* 125:163–172
- Patankar SV, Spalding DB (1972) A calculation procedure for heat, mass and momentum transfer in three-dimensional parabolic flows. *Int J Heat Mass Transfer* 15:1787–1805
- Rahimi M, Akbari M, Parsamoghadam MA, Alsairafi AA (2015) CFD study on effect of channel confluence angle on fluid flow pattern in asymmetrical shaped microchannels. *Comput Chem Eng* 73:172–182
- Rahimi M, Azimi N, Parsamoghadam MA, Rahimi A, Masahy MM (2017) Mixing performance of T, Y and oriented Y-micromixers with spatially arranged outlet channel: evaluation with Villermaux/Dushman test reaction. *Microcyst Technol* 23:3117–3130
- Sarkar S, Singh KK, Shankar V, Shenoy KT (2014) Numerical simulation of mixing at 1–1 and 1–2 microfluidic junctions. *Chem Eng Process* 85:227–240
- Soleymani A, Kolehmainen E, Turunen I (2008) Numerical and experimental investigations of liquid mixing in T-type micromixers. *Chem Eng J* 135:S219–S228
- Vatankhah P, Shamloo A (2018) Parametric study on mixing process in an in-plane spiral micromixer utilizing chaotic advection. *Anal Chim Acta* 1022:96–105
- Zhendong L, Yangcheng L, Jiawei W, Guangsheng L (2012) Mixing characterization and scaling-up analysis of asymmetrical T-shaped micromixer Experiment and CFD simulation. *Chem Eng J* 181–182:597–606

Publisher's Note Springer Nature remains neutral with regard to jurisdictional claims in published maps and institutional affiliations.